Broadband Bilayer Antireflective Coating with Metasurfaces and Chebyshev Transformer

Xiaojing Li,[1,2] Wuan Zheng,[2,3] Wenhao Zhang,[4] and Tong Hao◉[2,3,*]

[1]*School of Physics Science and Engineering, Tongji University, Shanghai 200092, China*

[2]*Center for Spatial Information Science and Sustainable Development Applications, Tongji University, Shanghai 200092, China*

[3]*College of Surveying and Geo-Informatics, Tongji University, Shanghai 200092, China*

[4]*College of Electronic and Information Engineering, Tongji University, Shanghai 200092, China*

Antireflection coatings with a broad relative bandwidth (RBW) and reduced electrical length are desirable for a variety of applications in the microwave frequencies. Here, we propose the design principle of bilayer metasurfaces with 100% RBW and subwavelength thickness based on the traditional Chebyshev transformer, with excellent agreement with our experimental validation for both transverse electric and magnetic polarizations. We utilize the multiple-beam interference theory to reveal the underlying mechanism of the preferred choices for nonresonant or weakly resonant metasurface unit cells. Being able to manipulate the transmissions and reflections within the bilayer structure, we further demonstrate the universality and sensitivity of the designs capable of providing near-unity microwave transmission from air into the full range of natural media, with prescribed RBW and reduced electrical length.

I. INTRODUCTION

Antireflection, i.e., eliminating the undesirable reflections at the interface between two media in the microwave frequency band, is of great importance for a variety of applications, such as nondestructive testing, through-the-wall radar, and many other impedance unmatched systems [1]. The impedance mismatch at the interface is governed by the refraction index contrast between these two media, and traditionally single or multiple layered dielectrics are designed as antireflection coatings to match the impedance. The single-layer antireflection coating is the simplest approach that requires a refractive index matching and a quarter wavelength thickness of the coating [2], but its working bandwidth is typically narrow. On the other hand, although multilayered antireflection coating brings a broader working bandwidth, it also leads to a larger coating thickness, making it infeasible for real-world applications especially in the gigahertz band. For instance, ground penetrating radar (GPR) with ultra wideband radiation is an electromagnetic technique currently in use for the detection and imaging of buried objects whose mainstream operating frequency is typically in the 10–5000 MHz range [3]. There are increasing demands for electrically thin and broadband antireflection designs.

In the past decade, the development of metasurfaces—two-dimensional equivalent of metamaterials—has enabled unprecedented capabilities in manipulating electromagnetic (EM) wave interaction with the media using an array of metal or dielectric unit cells [4]. They can be homogenized and described by retrieved macroscopic quantities such as relative permittivity (ε_r), relative permeability (μ_r), and refractive index (n) as the constituent unit cells at subwavelength scale [5,6]. They provide an effective leverage to alleviate the nonavailability of natural materials with the required n because of the independently tailored ε_r and μ_r. The underlying physics is their capability in introducing discontinuity across the interface by locally producing an abrupt leap in phase, amplitude, and even polarization of EM waves [7]. One has seen numerous applications such as absorbers [8], focusing lenses [9], invisibility cloaks [10,11], high-efficiency wave-plates [12–14], and metaholograms [15].

The original study by Chen describes how a metasurface manipulates reflection and transmission and achieves a reflection canceling effect with a thin structure (0.12λ), although in their implementation the relative bandwidth (RBW) is still quite narrow, about 15% [16]. Note that in this paper we calculate the RBW based on the same criteria of the reflectance smaller than 0.1. Kim *et al.* [17] reported that a metamaterial structure consisting of a one-dimensional subwavelength metal and air-gap grating can enable a maximum transmittance of 93.4%, with the experimental RBW limited to 58% and thickness of 0.25λ in free space. For multilayer designs, Huang *et al.* [18] proposed a bilayer structure capable

*tonghao@tongji.edu.cn

of realizing dual and broadband optical antireflection in the terahertz and midinfrared bands. Their RBW is about 38% with a structural thickness of 0.35λ. Im *et al.* [19] developed a universal impedance matching theory and experimentally demonstrated a sandwich structure based on dielectric metasurfaces that can provide zero reflection of microwaves with a total thickness of 0.53λ. Xue *et al.* [20] designed a bilayer Huygens' metasurface lens with near-unity transmission amplitude and Yang *et al.* [21] demonstrated their design capable of providing near-perfect microwave transmission through glass. These designs, however, only achieved antireflection at particular frequencies with quite a narrow bandwidth. More recently, with the aim to increase the EM energy transmission into an underground medium, we present a GPR demonstration using a single-layer antireflection coating with the RBW about 21% [22]. With the careful selection and tuning of the unit cells, we also propose a structure-optimized metasurface design with the experimental validation of a relatively broad RBW (44%) with a thickness of 0.15λ in the gigahertz band [23]. Despite these advancements, existing antireflection designs cannot be simultaneously broadband and electrically thin. The design of an ultra wideband and electrically thin metasurface is still an important objective for the GPR community where the RBW normally needs to be approximately 100% [24].

Here in this paper we propose a broadband antireflection coating by combining a Chebyshev transformer and metasurfaces with a reduced thickness compared with conventional coating designs. Because of experimental purposes and the requirements of the GPR application, we set the operating frequency at 2 GHz and the dielectric constant of the medium to be matched at 16. Based on the multibeam interference principle, we firstly design the Chebyshev transformer with the explicit RBW requirement. By imprinting the structurally optimized metallic claddings on the interface of each dielectric layer, we effectively manipulate the amplitude and phase of the EM reflections and transmissions to generate the antireflection behavior. Our designing objective and strategy are to reduce the electrical length of the single or multilayer dielectric coating while approaching the RBW limit prescribed by the Chebyshev transformer. By numerically evaluating and comparing the reflections of the strong and weakly resonant metasurface unit cells with the traditional Chebyshev transformer, it is carefully concluded that the key design principle for maintaining a broad antireflection bandwidth is nonresonance or weak resonance. A sensitivity analysis is also conducted for experimental validation of the proposed antireflection design, and this comprehensive numerical study on the broadband and electrically thin antireflection coating is the cornerstone for the practical implementation of impedance matching for a variety of media ranging from air to water.

II. DESIGN OF BROADBAND ANTIREFLECTION METASURFACES

A. Antireflection by multisection Chebyshev transformer

The single quarter-wave transformer is the simplest circuit for matching a load impedance to a transmission line if only a narrow band impedance match is required. Multisection quarter-wave transformer designs can be synthesized to yield optimum matching characteristics and provide broader bandwidth. There are two most commonly used passband responses: the binomial (maximally flat) response and the Chebyshev (equal-ripple) response [25]. The latter has a wider bandwidth that is optimized at the expense of passband ripples.

Utilizing the theory of small reflections [25], we can design a Chebyshev transformer to match air ($\varepsilon_0 = 1$) with the substrate ($\varepsilon_s = 16$) with a predefined number of sections N and the maximum allowable magnitude of the reflection coefficient Γ_m, as shown in Fig. 1(a). If not otherwise specified, relative permittivity is assumed in this paper. We start with the lossless scenario, before the losses of the substrate and the spacer are introduced in subsequent sections. The essence of designing a Chebyshev transformer is to equate the overall reflection coefficient Γ_θ to a Chebyshev polynomial $T_N (\sec \theta_m \cos \theta)$, where the total reflection is expressed as the sum of partial reflections at the material interface Γ_N,

$$
\begin{aligned}
\Gamma(\theta) &= 2e^{-jN\theta} \left[\Gamma_0 \cos N\theta + \Gamma_1 \cos (N-2)\theta + \cdots \right. \\
&\quad \left. + \Gamma_n \cos (N-2n)\theta + \cdots \right] \\
&= Ae^{-jN\theta} T_N (\sec \theta_m \cos \theta),
\end{aligned}
\tag{1}
$$

where the last term in the series is $(1/2)\Gamma_{N/2}$ for N even and $\Gamma_{(N-1)/2} \cos \theta$ for N odd. Here N is the number of sections, $\theta = kl$ is the electrical length of each section expressed in radians or the phase delay when the incident wave travels up and down the line, and θ_m is the lower passband edge in the transformer; $k = \omega \sqrt{\varepsilon_r \mu_r}$ is the wave number in the medium and l is the electrical length of the matching section. The transformer is symmetrical, so that $\Gamma_0 = \Gamma_N$, $\Gamma_1 = \Gamma_{N-1}$, and so on. Giving the value we set to $\Gamma_m = |A|$, θ_m can be determined as

$$
\sec \theta_m = \cosh \left[\frac{1}{N} \cosh^{-1} \left(\left| \frac{\ln Z_L/Z_0}{2|A|} \right| \right) \right].
\tag{2}
$$

The characteristic impedance Z_n of each layer can be found from

$$
\Gamma_N = \frac{1}{2} \ln \frac{Z_{n+1}}{Z_n}.
\tag{3}
$$

Once we obtain the impedance Z_n, the relative permittivity and the relative permeability of each layer can be

determined from $Z_n = \sqrt{\mu_n/\varepsilon_n}$ and $n_n = \sqrt{\mu_n\varepsilon_n}$, where we assume μ_n equals 1. The RBW, which is one of the key evaluation metrics in this study, can be calculated using

$$\frac{\Delta f}{f_0} = 2 - \frac{4\theta_m}{\pi}. \tag{4}$$

Combining Eqs. (2) and (4), we can obtain the RBW with an arbitrary Γ_m. Note that in this study we calculate RBW with reflectance R (≤ 0.1), while Γ_m is set at 0.1 for the design of the Chebyshev transformer. The electrical lengths of all sections in the conventional Chebyshev transformer are a quarter of the wavelength in the medium, at the working frequency 2 GHz, as shown in Fig. 1(a). Here Z_i represents the impedance of each layer, where the subscript "0", "1", "2", and "s" represent air, the first layer, the second layer, and the substrate to be matched, respectively. With $\Gamma_m = 0.1$, $N = 1$ and 2, we construct two metasurface coatings based on the Chebyshev transformer, as illustrated in Figs. 1(b) and 1(c), respectively. The yellow dotted lines are metallic metasurfaces that will be later demonstrated to reduce the electrical length of each section. For the single-layer coating, the physical length of the section is 18.75 mm, in which the permittivity is $\varepsilon_1 = 4$. For the bilayer coating, the physical lengths of the first and second section are 25.22 mm and 13.94 mm, with the corresponding $\varepsilon_1 = 2.21$ and $\varepsilon_2 = 7.24$, respectively.

We further study the mechanism of antireflection by analyzing the behavior of electromagnetic waves on different interfaces of the media using the multiple-beam interference theory [16]. Take the bilayer transformer as an example, we first treat the substrate and the second layer

as a single composite substrate layer, and then it is simplified into a single-layer transform problem, as shown in Fig. 1(d). The reflection of this equivalent system ($\widetilde{r}_{es}$) can be described as

$$\widetilde{r}_{es} = \frac{\widetilde{r}_{12} + \widetilde{r}_{23}e^{-2j\theta_2}}{1 + \widetilde{r}_{12}\widetilde{r}_{23}e^{-2j\theta_2}}. \tag{5}$$

As shown in Fig. 1(d), $\phi_{i,j}$ and $\theta_{i,j}$ are the reflection phase and the transmission phase, respectively. The partial reflection coefficient $\widetilde{r}_{i,j} = r_{i,j}e^{i\phi_{i,j}}$ and transmission coefficient $\widetilde{t}_{i,j} = t_{i,j}e^{i\theta_{i,j}}$ at the interface are used to compute the total reflection, which can be written in the same way as

$$\widetilde{r} = \frac{\widetilde{r}_{01} + \widetilde{r}_{es}e^{-2j\theta}}{1 + \widetilde{r}_{01}\widetilde{r}_{es}e^{-2j\theta}}, \tag{6}$$

where θ and θ_2 are the phase difference between two successive beams caused by an optical path difference in the first and second layer, respectively. Considering that $\widetilde{r}_{01} = (n_0 - n_1)/(n_0 + n_1)$, $\widetilde{r}_{10} = (n_1 - n_0)/(n_0 + n_1)$, $\widetilde{t}_{01} = 2n_0/(n_0 + n_1)$, and $\widetilde{t}_{10} = 2n_1/(n_0 + n_1)$, we have $\widetilde{r}_{01}^2 + \widetilde{t}_{01}\widetilde{t}_{10} = 1$. This allows us to describe the overall reflection as

$$\widetilde{r} = \frac{\widetilde{r}_{01} + \widetilde{r}_{es}e^{-2j\theta}\left(-\widetilde{r}_{01}\widetilde{r}_{10} + \widetilde{t}_{01}\widetilde{t}_{10}\right)}{1 - \widetilde{r}_{10}\widetilde{r}_{es}e^{-2j\theta}}. \tag{7}$$

If lossless media are assumed, the reflection can be simplified as

$$\widetilde{r} = \frac{r_{10}e^{i\phi_{01}} - r_{es}e^{i(\phi_{01} + \phi_{10} + \phi_{es} - 2\theta)}}{1 - r_{10}r_{es}e^{i(\phi_{10} + \phi_{es} - 2\theta)}}, \tag{8}$$
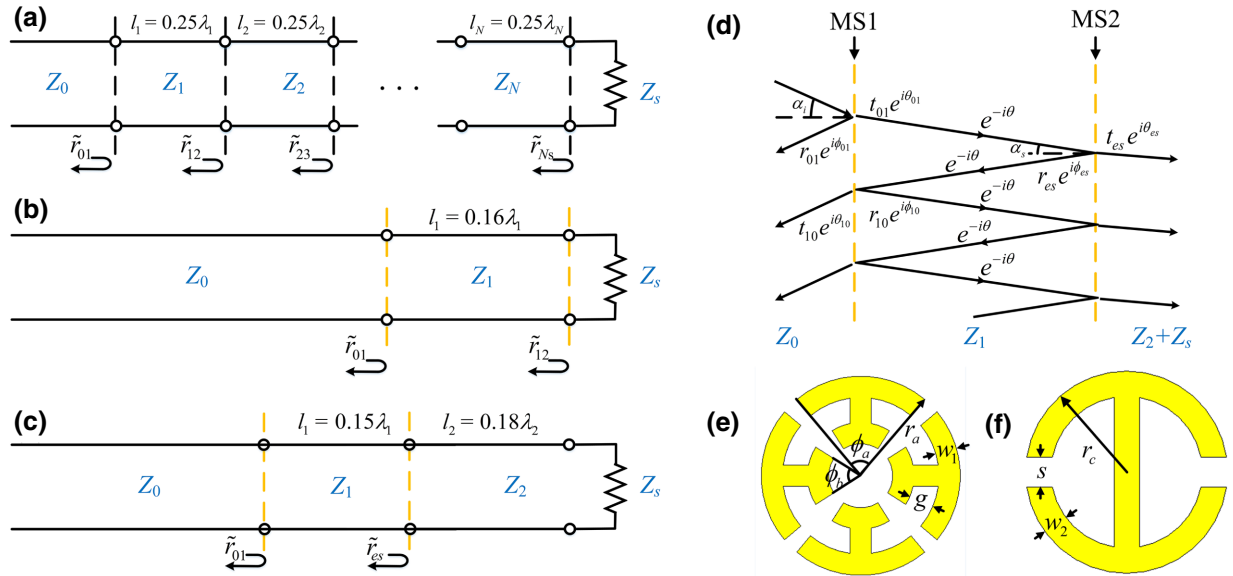

FIG. 1. Transmission line of (a) the multisection Chebyshev transformer, (b) the single-layer metasurface coating, and (c) the bilayer metasurface coating. (d) The principle of multibeam interference theory. (e),(f) Schematics of two metasurface unit cells consisting of two copper double split rings and one copper split ring with a bar, respectively.

which indicates that once conditions (i) $r_{01} = r_{10} = r_{es}$ and (ii) $\phi_{10} + \phi_{es} = 2\theta$ are both satisfied or approximately satisfied, antireflection can be obtained.

B. Design of the metasurface unit cell

Note that our design strategy is optimizing the metallic unit cells to reduce the electrical length of the spacer sections while maintaining the broadband antireflection achieved by the Chebyshev transformer. The metallic patterns are printed on the front side of each spacer section. The choice and structural optimization of such a pattern is of great importance in achieving antireflection [16,18,23], with varied performance in thinning the electrical length of the spacer [23]. Here we take our bilayer structure to illustrate this design progress, while the simple single-layer case can be found in Appendix A.

The commercially available package CST Studio Suite is used for the numerical simulations in the frequency domain, where the perfect electrical conducting boundary (*x* axis), perfect magnetic conducting boundary (*y* axis), and tetrahedral mesh are applied. The complete metasurface is the periodic extension of the unit cell in both X and Y directions, with a plane wave propagating along the z axis. As shown in Fig. 2(a), the parameters of the simulation model, l_{air} and l_{sub}, are set to 30 and 50 mm, respectively. With the calculated complex S parameters from the simulation results, we obtain the frequency dependent reflectance $R = |S_{11}|^2$, transmittance $T = |S_{21}|^2$, and

TABLE I. Key geometry parameters of different metasurfaces.

Metasurface	ϕ_a (°)	ϕ_b (°)	r_a (mm)	w_1 (mm)	g (mm)
MS1a	80	90	14.5	2	3.5
MS1b	60	90	13	2	3.5
MS1c	80	80	14	4	3.5
MS2a	90	90	11	3	1
MS2b	60	60	7	1	1
MS2c	80	60	10.5	3	2

absorbance $A = 1 - T - R$. We can also obtain the partial reflection coefficient r_{01}, r_{es}, ϕ_{01}, and ϕ_{es} by independently modelling MS1 and MS2 in Figs. 2(a) and 2(b), i.e., MS2, the second spacer section, and the substrate are removed from the unit cell for the MS1 interface, while air and MS1 are removed for the MS2 interface. It is obvious that r_{01} and ϕ_{01} are determined by MS1, while r_{es} and ϕ_{es} by MS2. Three MS1 variants, i.e., MS1a, MS1b, and MS1c, are applied in front of the first spacer section to obtain r_{01} and ϕ_{01}, and MS2a, MS2b, and MS2c are in front of the second spacer section to obtain r_{es} and ϕ_{es}, that are denoted by red, blue, and green solid lines in Figs. 2(c), 2(d), 2(f) and 2(g), respectively. The key geometrical parameters of these six variants are listed in Table I.

It is important to note that MS2c is applied in front of the second spacer section when we compare the MS1 variants for the first spacer section, while MS1c is fixed in front of the first spacer section when we compare
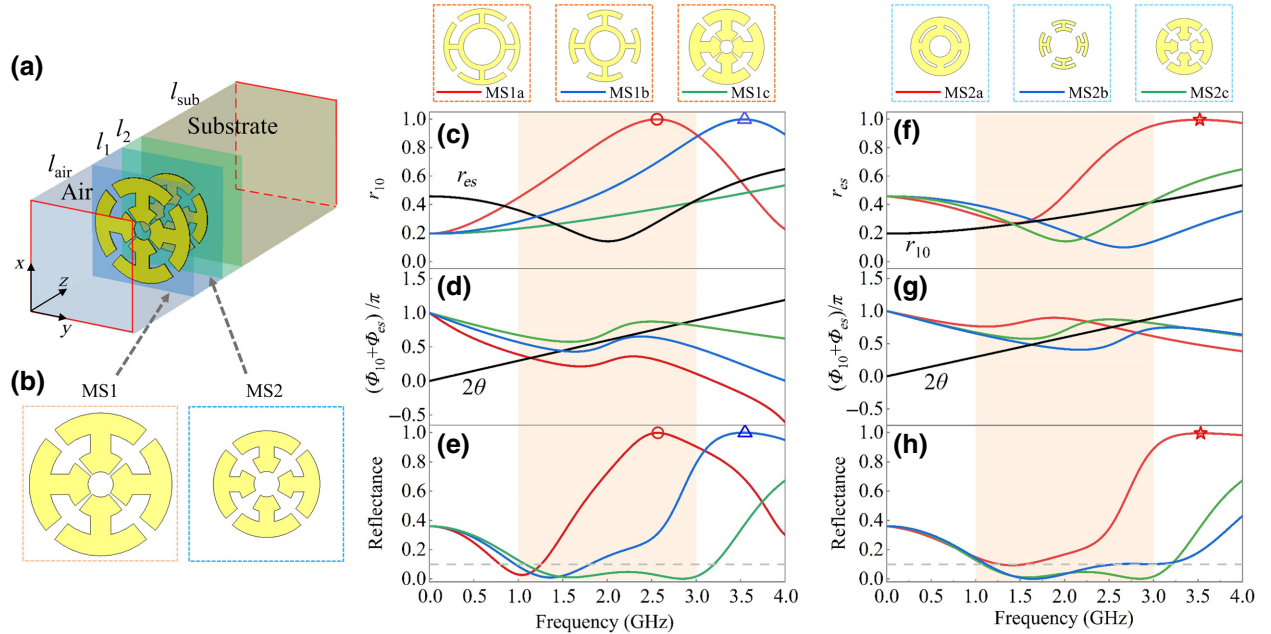

FIG. 2. Illustration of the numerical model (a) with two metasurfaces MS1 and MS2 (b) imprinted in front of each spacer section. Amplitude and phase conditions required for realizing broadband antireflection using six different metasurfaces. (c) Partial reflection r_{10}, (d) $\phi_{10} + \phi_{es}$, and (e) total reflectance obtained by full-wave numerical simulations for MS1a, MS1b, and MS1c imprinted on the $Z_0 - Z_1$ interface and MS2c fixed on the $Z_1 - Z_2$ interface. (f) Partial reflection r_{es}, (g) $\phi_{10} + \phi_{es}$, and (h) total reflectance for MS2a, MS2b, and MS2c imprinted on the $Z_1 - Z_2$ interface and MS1c fixed on the $Z_0 - Z_1$ interface.

TABLE II. The RMSE values of different metasurfaces.

RMSE	MS1a	MS1b	MS1c	MS2a	MS2b	MS2c
r_{10} and r_{es}	0.591	0.324	0.109	0.293	0.180	0.109
$(\phi_{10} + \phi_{es})$ and 2θ	0.377	0.155	0.159	0.297	0.202	0.159

MS2 variants for the second spacer section, with their response plotted as black solid lines. In order to measure how well the metasurface variants meet the antireflection conditions, the root-mean-square error (RMSE) is calculated to quantitatively evaluate the degree of similarity between the amplitudes (r_{10} and r_{es}), as well as the phases (($\phi_{10} + \phi_{es}$) and 2θ). As listed in Table II, it is clear that the combination of MS1c and MS2c provides the smallest RMSE, leading to the best antireflection, which is also evident in Figs. 2(e) and 2(h).

As prescribed in the previous design of the Chebyshev transformer, we aim for a RBW of approximately 103% with $\Gamma_m = 0.1$, which refers to the frequency range of 0.97–3.03 GHz with the center frequency of 2 GHz. MS1a shows a strong resonance denoted by the red hollow circle in Fig. 2(c), failing to satisfy the antireflection conditions across this frequency band. Furthermore, the resonance of MS1b is close enough to the frequency band of interest, unsatisfying the $r_{01} = r_{10} = r_{es}$ condition, although the $\phi_{10} + \phi_{es} = 2\theta$ condition is mostly met. The resonance of MS1c is the furthest from this frequency band or, in other words, shows the weakest resonance within the band, which is the underlying cause of a well-maintained broadband antireflection. Similar conclusions can be drawn for MS2 as witnessed in Figs. 2(f)–2(h), where the MS2 variant with weaker resonance within the frequency band leads to a broader antireflection. However, it is important to note that, compared with MS1, the resonance of r_{es}, which is affected by MS2, is more complex to analyze because the substrate and the second spacer section are considered as a composite. Because of the interference within this multilayer medium, we cannot simply attribute the peak and valley values of the r_{es} curve to the resonance response of MS2. Comparing Figs. 2(e) and 2(h), it is evident that the choice of a proper metasurface is vital in achieving broadband antireflection. More specifically, the existence of a strong resonance of a metasurface will sabotage the antireflection bandwidth while a unit cell with nonresonance or weak resonance is preferred. If the first spacer section is coated by MS1a, MS1b, and MS1c, with MS2c fixed for the second section, the RBW is calculated as 45.41%, 60.5%, 100%, respectively. If the second spacer section is coated by MS2a, MS2b, and MS2c, with MS1c fixed for the first section, the RBW is calculated as 0, 73.63%, 100%, respectively.

Based on the multiple-beam interference theory [16], a certain length of the dielectric spacer is needed for EM waves to interfere to satisfy the antireflection conditions.

The resonance of the imprinted metasurfaces is able to alter EM propagative behavior to tune for the balance of the interference. However, strong resonance would sabotage this delicate balance as shown in Figs. 2(e) and 2(h), and instead, the designed metallic metasurfaces in their nonresonant or weakly resonant mode exhibit effectively dielectric properties to incident electromagnetic waves, making the undesirable electromagnetic resonance response disappear.

III. RESULTS AND DISCUSSION

A. Thinning of broadband antireflection coating

We next demonstrate the advantage of a metasurface in thinning of our broadband antireflection spacer sections. As previously explained, the metasurfaces introduce field discontinuities across the section interfaces to locally produce phase manipulation, e.g., ϕ_{10} at the $Z_0 - Z_1$ interface. Obviously, when resonators are coated on the front side of the first layer, the amplitudes and corresponding phases of the reflection coefficients at this interface vary with frequency (although it is a weakly resonant structure in the desired frequency band, just like MS1c that we choose as the final unit cell in Fig. 2). Such phase changes are correlated to the electric and magnetic field distributions within the metasurface's metallic structure, and can be tuned by proper design and geometrical optimization to compensate for the electrical length of the dielectric section required for the cancellation of phase differences.

The progressive reduction of the electrical length of the spacer section by introducing metasurfaces at the section interfaces is provided in Fig. 3. The length of the first section decreases from 25.22 to 15 mm by applying MS1, if comparing the insets between Fig. 3(II-a) and Fig. 3(I-a). Therefore, the length dependent θ has an obvious decline in Fig. 3(II-b) compared with Fig. 3(I-b). However, the response of ϕ_{10} reduces with increased frequencies, so that $\phi_{10} + \phi_{es} = 2\theta$ can be satisfied and the antireflection range is almost unchanged in Fig. 3(I-c, II-c). This result demonstrates that MS1 can provide a length compensation through the manipulation of ϕ_{10}. More preciously, a 10.22 mm thick dielectric layer of $\varepsilon_1 = 2.21$ is safely replaced by a metasurface metallic structure whose thickness can be neglected.

As displayed in the inset of Fig. 3(III-a), MS2 is printed in front of the second section whose length is reduced from 13.94 to 10 mm. Although it is thinner, ϕ_{es} remains barely changed due to the weak resonance of MS2. Considering ϕ_{10} and θ are both the same as the traditional Chebyshev transformer, which are shown in Fig. 3(I-b, III-b), the phase condition is almost satisfied in the frequency range (1–3 GHz). Comparing Fig. 3(III-c) to Fig. 3 (I-c), a similar conclusion can be drawn that MS2c is equivalent to a dielectric spacer section with the length of 3.94 mm and $\varepsilon_2 = 7.24$. Finally, by applying MS1 and MS2 to
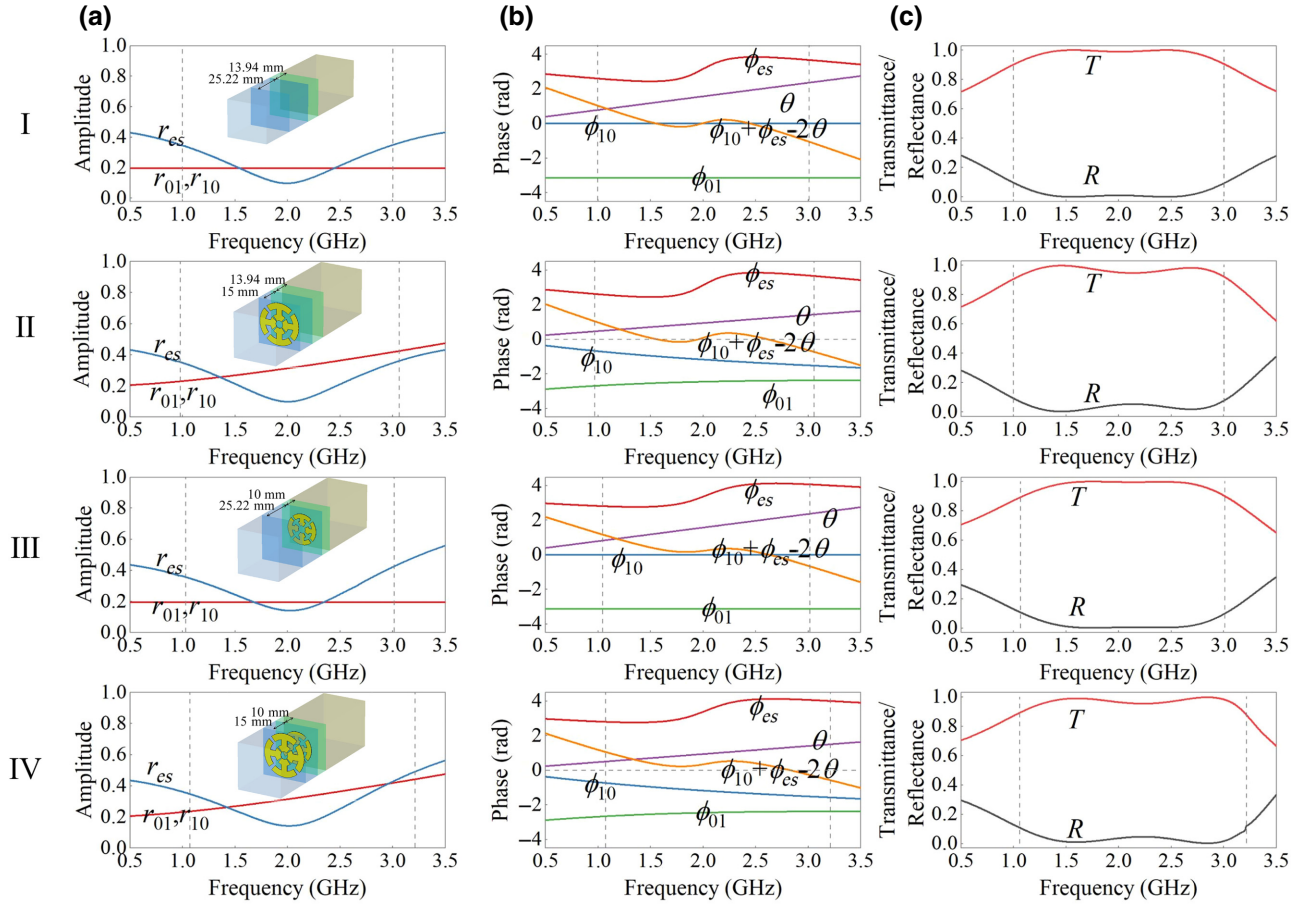
FIG. 3. Underlying mechanism of antireflection by the illustrations of (I-a) the bilayer Chebyshev transformer, (II-a) the transformer with MS1c imprinted on the front interface of the first section, (III-a) the transformer with MS2c imprinted on the front interface of the second section, and (IV-a) the bilayer coating with the imprinted MS1c and MS2c, with their (a) reflection amplitudes, (b) reflection phases, and (c) total transmittance and reflectance.

the front side of both the first and second sections of the Chebyshev transformer [see the inset in Fig. 3(IV-a)], we obtain the design with the thinnest electrical length in the frequency range between 1.07 and 3.22 GHz, with an ultra wideband RBW of 100%. This frequency range is slightly shifted from the previous Chebyshev transformer that is 0.97–3.03 GHz with RBW of 103%.

B. Validation study and discussion

We conduct the sensitivity analysis before our experimental validations, mainly considering the manufacturing errors of the proposed metasurface structures. Further details can be found in Appendix B. Based on the simulation results of Fig. 3(IV-a), a 20×20 array of metasurface unit cells are printed on the F_4B substrate with the size of $600 \times 600 \times 15$ mm^3 for the first layer (unit cell: MS1c) and $600 \times 600 \times 10$ mm^3 for the second layer (unit cell: MS2c), respectively. These two metasurface substrates are then assembled to form the bilayer sample structure and experimentally characterized in our microwave anechoic

chamber, as depicted in Fig. 4(a). We use two identical horn antennas to measure the transmission and reflection in the frequency range of 0.5–4 GHz. Aiming for the nondestructive testing applications, we use the presoaked foam brick as the medium to be matched, whose relative permittivity is settled the same as in previous simulations (approximately 16).

To eliminate all the ambient electromagnetic disturbance even within the microwave anechoic chamber, a four-step procedure is used for the reflectance measurement. First, S_{21} is measured as the complex amplitude of waves E_{direct} at the receiving antenna without any structure in the anechoic chamber. Second, we place the prepared moist foam brick in front of the antennas, and measure S_{21} to yield the reflection response $E_{\text{tot}}^{\text{sub}} = E_{\text{direct}} + E_{\text{refl}}^{\text{sub}}$. To prevent the near-field effects, we make sure that the foam brick and antennas are separated by a distance greater than D^2/λ. Here, D represents the largest transverse dimension of the antenna aperture and λ is the working wavelength. Third, we place an aluminum plate in front of the moist foam brick and measure S_{21} to obtain the total reflection
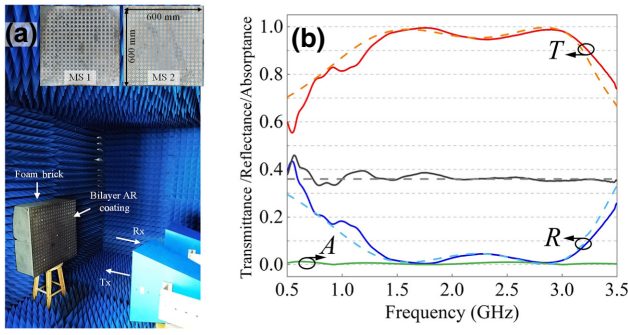
FIG. 4. (a) Photograph of the experiment setup in the ane-choic chamber with two metasurface sample insets. (b) Measurement results for the metasurface's absorbance (green solid line), reflectance (blue solid line), and calculated transmittance (red solid line). The reflectance curves of the bare substrate are represented by the dashed gray line for simulation results and gray solid line for measured results.

response $E_{tot}^{AL} = E_{direct} + E_{refl}^{AL}$. The reference amplitude of EM waves reflected by an aluminum plate, E_{refl}^{AL}, is used to normalize reflectance for all other measured signals with the same geometry. Finally, we replace the aluminum plate with the bilayer metasurface sample in front of the foam brick and measure the signal E_{tot}^{MS}. The reflectance of the bare foam brick and that of the foam brick with the antireflection metasurface coating can thus be calculated as

$$R_{sub} = \left|\frac{E_{refl}^{sub}}{E_{refl}^{AL}}\right|^2 = \left|\frac{E_{tot}^{sub} - E_{direct}}{E_{tot}^{AL} - E_{direct}}\right|^2, \qquad (9a)$$

$$R_{MS} = \left|\frac{E_{refl}^{MS}}{E_{refl}^{AL}}\right|^2 = \left|\frac{E_{tot}^{MS} - E_{direct}}{E_{tot}^{AL} - E_{direct}}\right|^2. \qquad (9b)$$

We cannot directly measure the transmittance at the back of the moist foam brick since the substrate–air interface would inevitably introduce an additional impedance mismatch. In addition, the transmission we care about occurs at the interface between the matching layer and the moist foam brick, and the interior of the substrate is beyond our control in the application scenarios. Here, we deduce the transmittance with the energy conservation law $T = 1 - R - A$, where A is obtained by calculating the metasurface losses via conducting the transmission and reflection measurement by placing the transmitting and receiving antennas on opposite sides of the metasurface sample.

As shown in Fig. 4, the dashed lines represent the simulated transmittance and reflectance under ideal lossless conditions, which also correspond to the curves in Fig. 3(IV-c). The measured reflectance in Fig. 4(b) shows that from 1.21 to 3.26 GHz, the antireflection RBW of 92% is accomplished with $R \leq 0.1$, demonstrating the ultra broadband antireflection behavior, which is also in good agreement with the simulated RBW of 100% (1.07–3.22

GHz). Note that the measurement accuracy, especially the reflectance and transmittance at low frequencies, may be influenced by the limited size of the microwave anechoic chamber, since the ambient low-frequency electromagnetic disturbance could not be fully removed.

So far we have only considered the broadband antireflection under the normal incidence. To explore the angular dependent reflectance spectra, the reflectance for transverse electric (TE) and transverse magnetic (TM) polarizations for the metasurface structure are presented in Fig. 5. For both wave propagating directions, the angle between the wave vector direction and the z direction changes from $0°$ to $60°$ with the interval of $5°$. In Fig. 5(a) we witness that, under our antireflection criteria ($R \leq 0.1$), the RBW in simulation is gradually reduced with the increasing TE angles, from 100% under the normal incidence to 84.76% at $45°$. On the contrary, as displayed in Fig. 5(b), the RBW in simulation is gradually enlarged with the increasing TM angles, from 101.37% at $20°$ to 112.02% at $40°$, before it reaches 162.89% at $60°$. The shrinking RBW under TE polarization may be explained by the fact that the reflectance gradually increases with the incident angle, since the magnitudes and phase shifts of the reflection and transmission coefficients at the $Z_0 - Z_1$ and $Z_1 - Z_2$ interfaces gradually change in comparison to those of normal incidence. It is primarily due to the fact that the magnetic field component parallel with the metasurface decreases as the incident angle increases. For the TM polarization, the reflectance minimum only slightly changes because the magnetic field vector remains parallel to the metasurface, and does not change with the increased incident angles
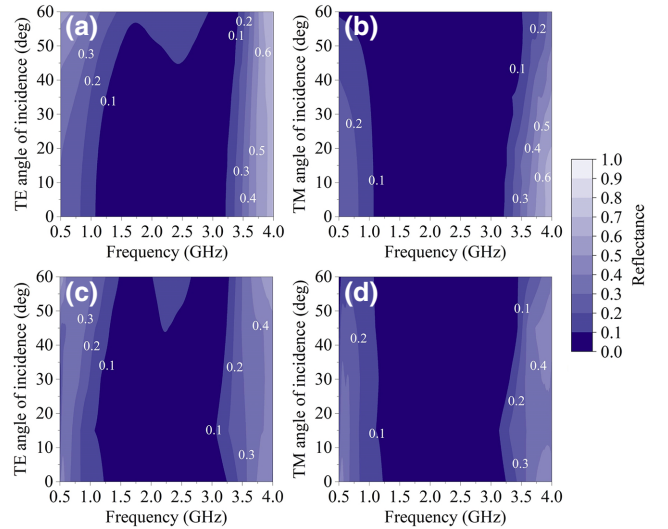

FIG. 5. Reflectance of the optimized bilayer antireflection coating under various angles of incidence for (a) TE and (b) TM polarizations in simulation, as well as for (c) TE and (d) TM polarizations by experiment.

[26,27]. Meanwhile, the frequency of the reflectance minimum barely shifts with the incident angles, and more frequencies of the reflectance satisfy our antireflection criteria ($R \le 0.1$) on either side of the reflectance minimum [16], resulting in the calculated RBW gradually expanding.

It is obvious that the reflectance for TE polarization is larger than that for TM polarization, particularly at increasing incidence angles. It is still significantly smaller than the reflectance relative to a bare substrate ($\varepsilon_s = 16$), which yields 0.36 (TE, TM) at the normal incidence, 0.38 (TE) and 0.34 (TM) at 20°, 0.46 (TE) and 0.26 (TM) at 40°, and 0.60 (TE) and 0.12 (TM) at 60°, respectively. In addition, this design is effective for both wave propagating directions, rather than only one direction antireflection with thin metal film coatings [28,29].

We perform the approximate Naval Research Laboratory (NRL) arch method to measure the reflection coefficients under various angles of incidence for TE and TM polarizations [30]. The incidence angles range from 0° to 60° with a step of 15°, which is restricted by the limited space of our anechoic chamber. Angular dependent reflectance spectra are directly measured and are shown in Figs. 5(c) and 5(d). One can see that the measured TE and TM reflectance spectra are in excellent agreement with the simulation results in Figs. 5(a) and 5(b).

C. Universality and outlook

Up to now, the proposed bilayer antireflection design has been thoroughly evaluated to match the air and substrate ($\varepsilon_s = 16$). This is based on the Chebyshev transformer with approximately 103% RBW, and the introduced metasurfaces effectively replace part of the transmission line's length.

Here we show the formula for how to combine the design of the Chebyshev transformer with metasurfaces to optimize a thinner and broadband bilayer antireflection coating. First, we design a two section Chebyshev transformer to match air with the target medium and this, as a result, defines the respective permittivity and thickness of the two matching layers. The physical lengths of the two sections are both one-quarter wavelength in each medium, as displayed in Fig. 3(I). Second, we optimize the metasurface unit cells, which are etched onto the front side of the first matching layer, by the parametric sweep of several key parameters in Table I. An optimized set of structural parameters reduce the layer thickness. In the structural optimization, we choose nonresonant or weakly resonant unit cells in the frequency band of interest, because a strong resonance in or immediately adjacent to the target frequency band would sabotage the broad bandwidth, e.g., MS1a and MS1b in Figs. 2(c) and 2(e). On the contrary, the weakly resonant unit cell MS1c demonstrates a better satisfaction of the antireflection amplitude condition (i) $r_{01} = r_{10} = r_{es}$. According to the phase condition

(ii) $\phi_{10} + \phi_{es} = 2\theta$, we select the metasurface unit cell with the smallest ϕ_{10} among weakly resonant unit cell candidates to obtain the thinnest layer since θ is directly proportional to the layer thickness. These two optimization criteria, which correspond to both antireflection conditions, can assist us in determining the suitable metasurface structure. Third, we thin out the second layer by applying an optimized metallic metasurface at the $Z_1 - Z_2$ interface. As shown in Figs. 2(f)–2(h), the optimization criteria are similar to the second step above, except that here we consider the substrate and the second section layer as one whole behind the metallic metasurface. We need to ensure that the values of r_{es} and ϕ_{es} are as close to the Chebyshev transformer as possible, after introducing the metasurface for the second layer, as seen in Figs. 3(III) and 3(I). Finally, two optimized metallic metasurfaces are simultaneously applied in front of the corresponding dielectric layer to yield a broadband thin antireflection coating with RBW only slightly different from that defined by the classical Chebyshev transformer.

Such a design procedure can be extended to match air to a variety of materials with permittivity up to 81, as shown in Fig. 6. For $\varepsilon_s = 16$, as discussed above, the physical length of the metasurface antireflection coating is 25 mm, with a significant reduction of approximately 36.2% compared with the conventional antireflection based on the Chebyshev transformer (39.2 mm), while the RBW is sustained around approximately 100%. For the single-layer coating case (see Appendix A), the reduction of the physical length is approximately 36%, with RBW being changed from 60% to 65%. For materials with high permittivities, such as $\varepsilon_s = 36$ and $\varepsilon_s = 64$, the physical length reductions of approximately 27.5% (33.1 to
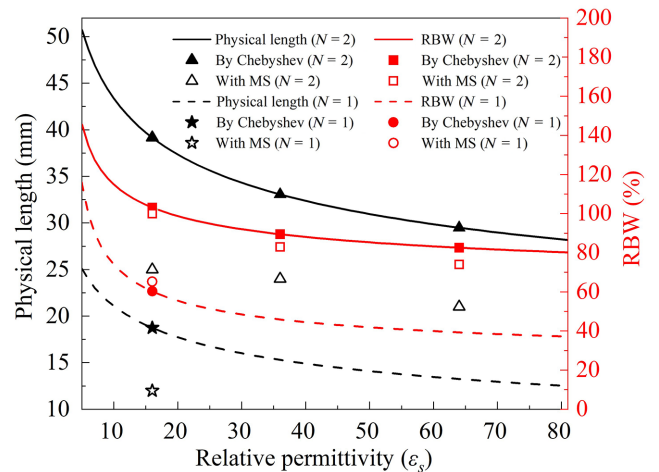

FIG. 6. The physical length and RBW of the traditional Chebyshev transformer (center frequency, 2 GHz) and metasurface antireflection coating for a large range of the relative permittivity ($5 \le \varepsilon_s \le 81$) with the matching section numbers $N = 1$ and $N = 2$.

TABLE III. Comparison between our proposed design and previously demonstrated single-layer and multi-layer metasurfaces.

Ref.	RBW (%)	Total electrical length (λ)	Target Permittivity (ϵ_s)	Type
16	15	0.12	12.7	Single layer
17	58	0.25	16	Single layer
18	38	0.35	11.56	Bilayer
19	$\cdots$	0.53	2.25	Bilayer
21	$\cdots$, narrow band	0.08	6.5	Triple layer
22	21	0.07	15	Single layer
23	44	0.15	15	Single layer
This work	65	0.16	16	Single layer
This work	100	0.33	16	Bilayer

24 mm) and approximately 26.3% (28.5 to 21 mm) are observed, respectively, for a bilayer metasurface antireflection coating; however, the RBW is inevitably deteriorated. Although the physical length decreases with higher ε_s, the corresponding RBW decreases too, restricting its feasibility for ultra wideband applications. One may increase the number of sections to improve RBW, however, the physical length will inevitably increase. Therefore, challenges still exist for the design of electrically thin and broadband coatings for materials with full range ε_s, where the balance between the electrical length and RBW must be carefully tailored.

Finally, we compare our single-layer and bilayer designs with previous metasurface demonstrations [16–19,21–23] in Table III, and manifest that, for the bilayer cases, our RBW is increased by more than 160%, and approaching the bandwidth limit governed by the design principle of multisection transformers [25]. This is also true for the single-layer cases, and compared with various existing studies, our design witnesses the largest RBW and highest target permittivity to match with the electrical length in the deep subwavelength scale.

IV. CONCLUSION

By combining structurally optimized metasurfaces to each layer of the traditional Chebyshev transformer, we design a bilayer antireflection coating with approximately 100% RBW ($R \leq 0.1$) and 0.33λ thickness. We successfully explore the broadband mechanism that the metasurface shall have nonresonance or weak resonance. The metasurfaces at the bilayer interfaces effectively compensate the layer thickness required for the destructive interference of internal and interlayer transmissions and reflections. Our sensitivity studies verify the robustness of our designs to the dielectric uncertainties during the manufacturing process, paving the route for experimental validations. The measurements of ultra broadband antireflection coatings agree remarkably well with our simulations, and demonstrate excellent matching characteristics in the designed frequency band. Following the Chebyshev transformer, our bilayer design can be extended to match materials with a relative permittivity as high as water, with the distinct advantage of shrinking the overall electrical length. Furthermore, for higher frequency bands,
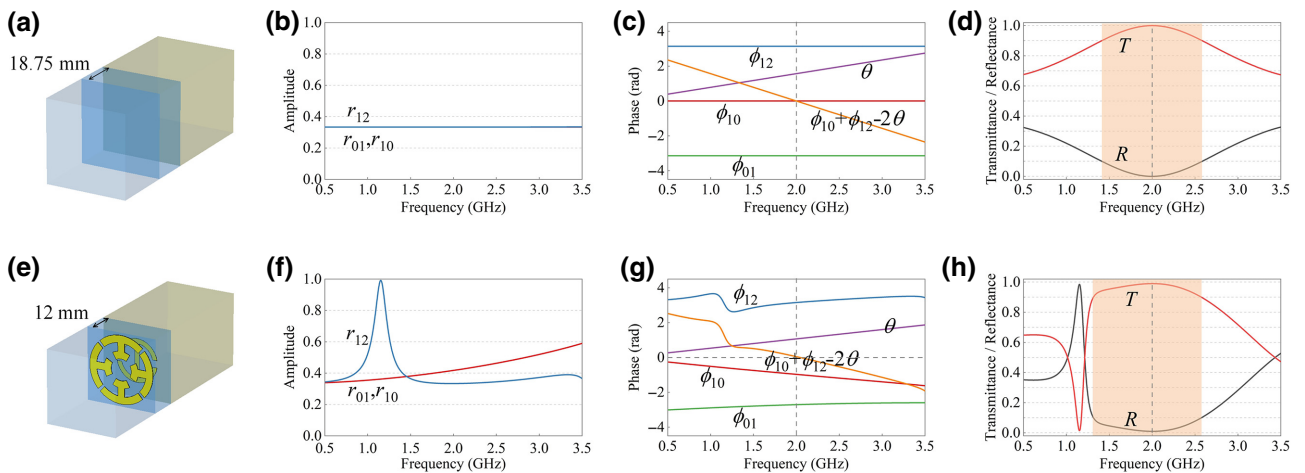

FIG. 7. Single-layer antireflection by (a) the traditional Chebyshev transformer and (e) the metasurface with reduced electrical length, with their (b),(f) reflection amplitudes, (c),(g) reflection phases, and (d),(h) total reflectance and transmittance, respectively.
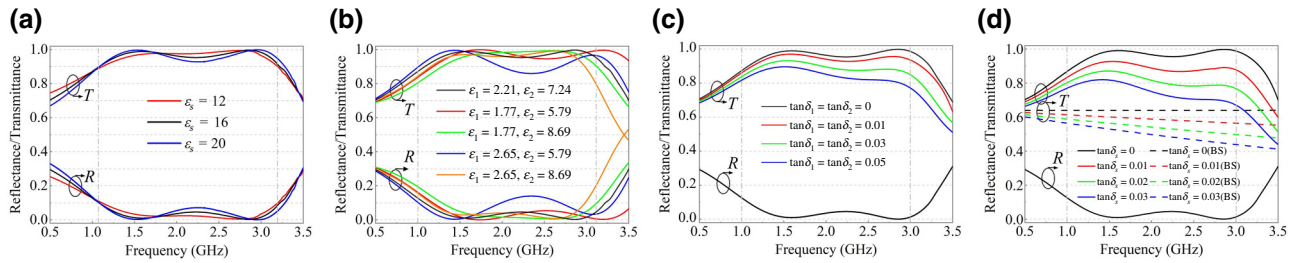
FIG. 8. Simulated reflectance and transmittance under the normal incidence with varied permittivity of (a) the substrate ($\pm 25\%$) and (b) the spacer sections ($\pm 20\%$); with a varied loss tangent of (c) the spacer sections (0 to 0.05) and (d) the substrate (0 to 0.03). (Here BS denotes bare substrate.)

such as millimetric band or even terahertz band, the proposed broadband design strategy shall have even more diverse application potentials.

APPENDIX A: SINGLE-LAYER ANTIREFLECTION COATING

As displayed in Fig. 7(a), the quarter wavelength single-layer antireflection coating is the most simple Chebyshev transformer whose physical length is 18.75 mm. After applying two optimized metasurfaces, the thickness reduces 12 mm (0.16λ) while the RBW (65%) is even better than before (60%) (Fig. 6) under the criterion of $R \leq 0.1$, as compared in Figs. 7(d) and 7(h). Two metasurface unit cells, which are imprinted on both sides of the spacer, are displayed in Figs. 1(e) and 1(f). The optimized parameters of the metasurface unit cell are $\phi_a = 85°$, $\phi_b = 60°$, $r_a = 14$ mm, $r_c = 9$ mm, $w_1 = 3$ mm, $w_2 = 2$ mm, $g = 3.5$ mm, and $s = 3$ mm. It is clear that good matching performance is maintained over the antireflection frequency range and zero reflectance is also achieved at 2 GHz with a thinner layer thickness. As shown in Figs. 7(f) and 7(g), as MS1 is introduced at the $Z_0 - Z_1$ interface, ϕ_{10} is no longer zero [Fig. 7(c)], but reduces with frequency, while r_{01} and r_{10} increases with frequency. With the optimized MS2 applied at the $Z_1 - Z_2$ interface, although a strong resonance appears around 1.2 GHz, r_{12} can be tuned to be approximately equal to r_{01} at 2 GHz. In the meantime, according to the phase condition $\phi_{10} + \phi_{12} = 2\theta$ and that θ is correlated to the layer thickness, the decrease of $(\phi_{10} + \phi_{12})$ directly leads to the reduced layer thickness. For the single-layer antireflection coating, we numerically demonstrate the structure with the highest RBW while maintaining a deep subwavelength electrical length.

APPENDIX B: SENSITIVITY ANALYSIS

We firstly evaluate the robustness of our numerically optimized bilayer design for the variance of the permittivity ($\pm 25\%$) of the substrate, as shown in Fig. 8(a). It is clear that in this lossless case all the transmittances are above 90% in the broadband frequency range. Exhibited in Fig. 8(b), the permittivity of each spacer section is varied by $\pm 20\%$, the majority of reflectance is smaller than 0.1, except the combination of $\varepsilon_1 = 2.65$ and $\varepsilon_2 = 5.79$. It is also interesting to see that such permittivity variance in each section leads to considerable RBW changes, where the combination of $\varepsilon_1 = 1.77$ and $\varepsilon_2 = 5.79$ results in an even wider RBW (102%).

Figures 8(c) and 8(d) display the sensitivity of the reflectance and transmittance to $\tan\delta_1$, $\tan\delta_2$, and $\tan\delta_s$, if the loss of the spacer sections and substrate are considered. When the loss tangent for the first and second spacer section varies from 0.01 to 0.05 [Fig. 8(c)], although the corresponding transmittance decreases accordingly, they are all higher than approximately 80% for 1–3 GHz. If only the loss in the substrate is considered, and as $\tan\delta_s$ varies from 0 to 0.03 [Fig. 8(d)], although the transmittance inevitably drops, e.g., to 0.67 at 3 GHz for $\tan\delta_s = 0.03$, the antireflection coating with our metasurface cladding (solid lines) provides an overall increase of at least 0.2 in transmittance, if compared with the bare substrate (dashed lines). Such transmittance improvement is more pronounced for the substrate with smaller losses and, for the lossless case, the improvement is more than 0.3.

[1] J. W. Strutt, On the intensity of light reflected from certain surfaces at nearly perpendicular incidence, Proc. R. Soc. Lond. **41**, 275 (1887).

[2] M. Born and E. Wolf, *Principles of Optics: Electromagnetic Theory of Propagation, Interference and Diffraction of Light* (Elsevier, Amsterdam, 2013).

[3] W. Wai-Lok Lai, X. Dérobert, and P. Annan, A review of ground penetrating radar application in civil engineering: A 30-year journey from locating and testing to imaging and diagnosis, NDT E Int. **96**, 58 (2018).

[4] P. Yeh and M. Hendry, Optical waves in layered media, Phys. Today **43**, 77 (1990).

[5] G. V. Eleftheriades and K. G. Balmain, *Negative-Refraction Metamaterials: Fundamental Principles and Applications* (John Wiley & Sons, Hoboken, 2005).

[6] R. Liu, T. J. Cui, D. Huang, B. Zhao, and D. R. Smith, Description and explanation of electromagnetic behaviors in artificial metamaterials based on effective medium theory, Phys. Rev. E **76**, 026606 (2007).

[7] N. Yu, P. Genevet, M. A. Kats, F. Aieta, J.-P. Tetienne, F. Capasso, and Z. Gaburro, Light propagation with phase discontinuities: Generalized laws of reflection and refraction, Science **334**, 333 (2011).

[8] N. I. Landy, S. Sajuyigbe, J. J. Mock, D. R. Smith, and W. J. Padilla, Perfect Metamaterial Absorber, Phys. Rev. Lett. **100**, 207402 (2008).

[9] X. Chen, M. Chen, M. Q. Mehmood, D. Wen, F. Yue, C.-W. Qiu, and S. Zhang, Longitudinal multifoci metalens for circularly polarized light, Adv. Opt. Mater. **3**, 1201 (2015).

[10] R. Liu, C. Ji, J. J. Mock, J. Y. Chin, T. J. Cui, and D. R. Smith, Broadband ground-plane cloak, Science **323**, 366 (2009).

[11] J. Yang, C. Huang, X. Wu, B. Sun, and X. Luo, Dual-wavelength carpet cloak using ultrathin metasurface, Adv. Opt. Mater. **6**, 1800073 (2018).

[12] Y.-H. Hu, S.-c. Jiang, Z.-H. Wang, X. Xiong, R.-W. Peng, and M. Wang, in *CLEO: QELS_Fundamental Science* (Optical Society of America, 2016), p. FM3N–6.

[13] F. Ding, Z. Wang, S. He, V. M. Shalaev, and A. V. Kildishev, Broadband high-efficiency half-wave plate: A supercell-based plasmonic metasurface approach, ACS Nano **9**, 4111 (2015).

[14] Y. Yang, W. Wang, P. Moitra, I. I. Kravchenko, D. P. Briggs, and J. Valentine, Dielectric meta-reflectarray for broadband linear polarization conversion and optical vortex generation, Nano Lett. **14**, 1394 (2014).

[15] L. Huang, X. Chen, H. Mühlenbernd, H. Zhang, S. Chen, B. Bai, Q. Tan, G. Jin, K.-W. Cheah, and C.-W. Qiu, *et al.*, Three-dimensional optical holography using a plasmonic metasurface, Nat. Commun. **4**, 1 (2013).

[16] H.-T. Chen, J. Zhou, J. F. O'Hara, F. Chen, A. K. Azad, and A. J. Taylor, Antireflection Coating Using Metamaterials and Identification of Its Mechanism, Phys. Rev. Lett. **105**, 073901 (2010).

[17] W. Kim, J. Guo, and J. Hendrickson, Subwavelength metal grating metamaterial for polarization-selective optical

antireflection coating, J. Opt. Soc. Am. B **32**, 1392 (2015).

[18] L. Huang, C.-C. Chang, B. Zeng, J. Nogan, S.-N. Luo, A. J. Taylor, A. K. Azad, and H.-T. Chen, Bilayer metasurfaces for dual- and broadband optical antireflection, ACS Photonics **4**, 2111 (2017).

[19] K. Im, J.-H. Kang, and Q.-H. Park, Universal impedance matching and the perfect transmission of white light, Nat. Photo. **12**, 143 (2018).

[20] C. Xue, Q. Lou, and Z. N. Chen, Broadband double-layered Huygens' metasurface lens antenna for 5G millimeter-wave systems, IEEE Trans. Antennas Propag. **68**, 1468 (2020).

[21] F. Yang, B. O. Raeker, D. T. Nguyen, J. D. Miller, Z. Xiong, A. Grbic, and J. S. Ho, Antireflection and Wavefront Manipulation with Cascaded Metasurfaces, Phys. Rev. Appl. **14**, 064044 (2020).

[22] T. Hao, W. Zheng, W. He, and K. Lin, Air-ground impedance matching by depositing metasurfaces for enhanced GPR detection, IEEE Trans. Geosci. Remote Sens. **58**, 4061 (2020).

[23] T. Hao, W. Zheng, W. Wang, Y. Zhou, J. Bai, K. Lin, and Z. Yu, Electrically thin metasurface for broadband transmission enhancement by manipulating the amplitude and phase of the reflection coefficients, J. Appl. Phys. **126**, 025303 (2019).

[24] D. J. Daniels, *Ground Penetrating Radar* Vol. 1 (IET, Futures Place, 2004).

[25] D. M. Pozar, *Microwave Engineering* (John Wiley & Sons, Hoboken, 2011).

[26] D. Wen, X. Huang, L. Guo, H. Yang, S. Han, and J. Zhang, Quadruple-band polarization-insensitive wide-angle metamaterial absorber based on multi-layer structure, Optik **126**, 1018 (2015).

[27] H. Cory and C. Zach, Wave propagation in metamaterial multi-layered structures, Microwave Opt. Technol. Lett. **40**, 460 (2004).

[28] J. Kröll, J. Darmo, and K. Unterrainer, Metallic wave-impedance matching layers for broadband terahertz optical systems, Opt. Express **15**, 6552 (2007).

[29] A. Thoman, A. Kern, H. Helm, and M. Walther, Nanostructured gold films as broadband terahertz antireflection coatings, Phys. Rev. B **77**, 195405 (2008).

[30] R. Biscaro, E. Nohara, G. Peixoto, R. Faez, and M. Rezende, in *Proceedings of the 2003 SBMO/IEEE MTT-S International Microwave and Optoelectronics Conference*, Vol. 1 (2003), p. 355.